Available online at www.sciencedirect.com
ScienceDirect
International Journal of Heat and Mass Transfer 50 (2007) 2208–2216
International Journal of HEAT and MASS TRANSFER
www.elsevier.com/locate/ijhmt

Double-pass flow heat transfer in a parallel-plate channel for improved device performance under uniform heat fluxes

Chii-Dong Ho *, Yu-Jui Chuang, Jr-Wei Tu

Department of Chemical and Materials Engineering, Tamkang University, Tamsui, Taipei 251, Taiwan, ROC

Received 14 August 2006; received in revised form 28 October 2006
Available online 22 December 2006

Abstract

A design of inserting in parallel an impermeable sheet to divide an open conduit into two subchannels for conducting double-pass laminar countercurrent operations under uniform heat fluxes, resulting in substantially improved the heat-transfer rate, has been designed and investigated theoretically by using an eigenfunction expansion in terms of power series for the homogeneous part and an asymptotic solution for the non-homogeneous part. The theoretical results of heat-transfer efficiency enhancement in double-pass parallel-plate heat exchangers are represented graphically and compared with those in the single-pass operations without an impermeable sheet inserted. The influence of the impermeable-sheet location on the heat-transfer efficiency enhancement as well as on the power consumption increment in double-pass operations has also been delineated.

Keywords: Heat transfer; Parallel-plate channel; Double-pass operation; Uniform heat fluxes; Conjugated Graetz problems

1. Introduction

Most of the interest devoted to the heat transfer in engineering applications is the study of the thermal response of the conduit wall and fluid temperature distributions to the two cases of the uniform wall temperature (Dirichlet problem) and uniform heat flux (Neumann problem). The system at steady state with laminar flow of the negligible axial conduction in cylindrical and parallel-plate geometries is known as the classical Graetz problem [1–3]. Michelsen and Villadsen [4], Papoutsakis et al. [5], Weigand [6] and Bilir [7] examined the effects of axial conduction for laminar flow inside conduit for low Prandtl number fluids, as referred to the extended Graetz problem. Moreover, Papoutsakis and Ramkrishna [8,9], Bernier and Baliga [10], Amin and Khan [11] and Yin and Bau [12] analyzed the conjugated Graetz problem with two or more contiguous phases or streams.

Analytical treatment of Graetz and conjugated Graetz problems for laminar flow is mainly based on the eigenfunction expansion technique in terms of power series in the noted studies [13–16]. The solution of conjugated Graetz problems is obtained successfully by solving the Sturm–Liouville systems and consequently the solution expressed in the form of the infinite series consisting of the eigenvalue associated with each eigenfunction. The alternative configuration with the recycle-effect concept leads to improve the heat-transfer efficiency enhancement due to increasing the flow rate of fluid and applies to many separation processes [17,18] and chemical reactors [19,20].

There are many studies [21–24] devoted to the heat-transfer problem in a parallel-plate channel. The present study is an extension of our previous work [16] to apply the case of the Neumann boundary condition for the conjugated Graetz problem of which the heat fluxes at the walls were specified. The surface resistant along the flow path, as expressed in the wall Nusselt number, could be a straightforward manner to analyze the heat-transfer efficiency of multistream or multiphase problems coupling

* Corresponding author. Fax: +886 2 26209887.
E-mail address: cdho@mail.tku.edu.tw (C.-D. Ho).

0017-9310/$ - see front matter © 2006 Elsevier Ltd. All rights reserved.
doi:10.1016/j.ijheatmasstransfer.2006.10.039

Nomenclature

B	conduit width, m
D_e	equivalent diameter of the conduit, m
d_{mn}	coefficient in the eigenfunction $F_{a,m}$
e_{mn}	coefficient in the eigenfunction $F_{b,m}$
F_m	eigenfunction associated with eigenvalue λ_m
f	friction factor
G_m	function defined during the use of orthogonal expansion method
Gz	Graetz number, $VW/\alpha BL$
H	defined by Eqs. (20) and (21)
$\bar{h}$	average heat-transfer coefficient, kW/m K
I_h	heat-transfer enhancement based on single-pass devices, defined by Eq. (57)
I_p	power consumption increment of, defined by Eq. (59)
L	conduit length, m
ℓw_f	friction loss in conduit, N m/kg
$\overline{Nu}$	average Nusselt number
P	power consumption, N m/s
q''	heat flux on the wall, J/m^2 s
Re	Reynolds number
S_m	expansion coefficient associated with eigenvalue λ_m
V	input volume flow rate of conduit, m^3/s
v	velocity distribution of fluid, m/s
$\overline{v}$	average velocity of fluid, m/s
W	conduit height, m
x	transversal coordinate, m
z	longitudinal coordinate, m

Greek symbols

α	thermal diffusivity of fluid, m^2/s
α_1	constant defined by Eq. (20)
α_2	integration constants in Eq. (22)
α_3	integration constants in Eq. (22)
β_1	constant defined by Eq. (21)
β_2	integration constants in Eq. (23)
β_3	integration constants in Eq. (23)
Δ	impermeable-sheet location
δ	impermeable-sheet thickness, m
η	transversal coordinate, x/W
θ	defined by Eq. (12)
λ_m	eigenvalue
μ	fluid viscosity, kg/m s
ξ	longitudinal coordinate, $z/(LGz)$
ρ	fluid density, kg/cm^3
ϕ	defined by Eq. (12)
ψ	dimensionless temperature, $k(T - T_I)/q''W$
$\overline{\psi}$	dimensionless bulk temperature

Subscripts

a	subchannel a
b	subchannel b
F	at the outlet
I	at the inlet
L	at the end of the channel
0	in a single-pass device without recycle
w	at the wall surface

mutual conditions at the interface. The purposes of the present study are (a) to obtain the wall temperature distribution in the axial direction under uniform wall heat fluxes based the superposition technique; (b) to study the device performance improvement in double-pass parallel-pate laminar countercurrent heaters or coolers by inserting an impermeable sheet in parallel; (c) to discuss the influence of the impermeable-sheet location on the heat-transfer efficiency enhancement. The solution methodology developed here in a simple form for a double-pass parallel-pate heater or cooler is made on the general treatment which can be applied to the heat- and mass-transfer problem of any arbitrary wall heat flux distribution or wall temperature distribution with more general geometry and it is the value of the present work.

2. Temperature distributions

An impermeable sheet is inserted into a parallel-plate heat exchanger to divide an open duct with height W, length L, and width B into two subchannels a and b as show in Fig. 1. The thickness of the impermeable sheet is δ and compared to the height W, it can be neglected, say $\delta \ll W$. The fluid with volumetric flow rate V and temperature T_I firstly feeds into subchannel a and then, the fluid was pumped into subchannel b at the end of the conduit with the aid of a convectional pump. The fluid is well mixed at the inlet and the outlet of each subchannel.

To simply the problem, the following assumptions are made: constant physical properties of fluid; fully-developed laminar flow in each subchannel; neglecting the entrance length and longitudinal heat conduction; ignoring the end effects and the thermal resistance of the impermeable sheet. With the aid of these assumptions, the energy balance equations of a double-pass heat exchanger with constant heat flux were formulated and written as

$$\frac{\partial^2 \psi_a(\eta_a,\xi)}{\partial \eta_a^2} = \left(\frac{v_a(\eta_a)W_a^2}{\alpha LGz}\right)\frac{\partial \psi_a(\eta_a,\xi)}{\partial \xi} \tag{1}$$

$$\frac{\partial^2 \psi_b(\eta_b,\xi)}{\partial \eta_b^2} = \left(\frac{v_b(\eta_b)W_b^2}{\alpha LGz}\right)\frac{\partial \psi_b(\eta_b,\xi)}{\partial \xi} \tag{2}$$

where v_a and v_b are the velocity distributions in subchannels a and b, respectively, and they are

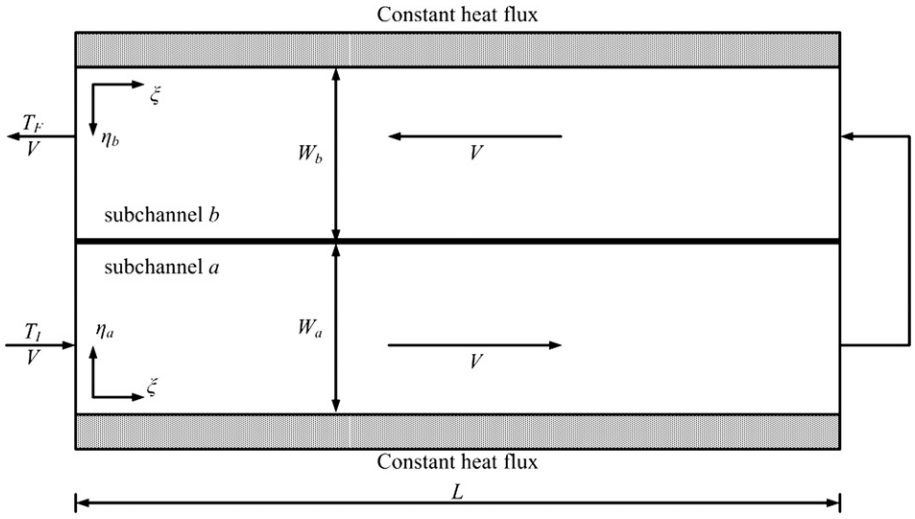

Fig. 1. Double-pass parallel-plate heat exchanger.

$$v_a(\eta_a) = \overline{v}_a(6\eta_a - 6\eta_a^2) \quad 0 \leqslant \eta_a \leqslant 1 \tag{3}$$

$$v_b(\eta_b) = -\overline{v}_b(6\eta_b - 6\eta_b^2) \quad 0 \leqslant \eta_b \leqslant 1 \tag{4}$$

$$\overline{v}_a = V/\Delta WB \tag{5}$$

$$\overline{v}_b = V/(1-\Delta)WB \tag{6}$$

The dimensionless groups in Eqs. (1)–(6) are

$$\eta_a = \frac{x_a}{W_a}, \quad \eta_b = \frac{x_b}{W_b}, \quad \xi = \frac{z}{LGz}, \quad Gz = \frac{VW}{\alpha BL},$$

$$\psi_a = \frac{k(T_a - T_I)}{q''W}, \quad \psi_b = \frac{k(T_b - T_I)}{q''W},$$

$$\Delta = \frac{W_a}{W}, \quad 1-\Delta = \frac{W_b}{W} \tag{7}$$

and the corresponding boundary conditions are

$$\frac{\partial \psi_a(0,\xi)}{\partial \eta_a} = -\Delta \tag{8}$$

$$\frac{\partial \psi_b(0,\xi)}{\partial \eta_b} = -(1-\Delta) \tag{9}$$

$$\psi_a(1,\xi) = \psi_b(1,\xi) \tag{10}$$

$$\frac{\partial \psi_a(1,\xi)}{\partial \eta_a} = -\frac{\Delta}{1-\Delta}\frac{\partial \psi_b(1,\xi)}{\partial \eta_b} \tag{11}$$

In order to remove the inhomogeneous boundary conditions (Eqs. (8) and (9)), the linear superposition of an asymptotic solution, $\theta(\eta,\xi)$, and a homogeneous solution, $\phi(\eta,\xi)$ is made and the complete solutions of Eqs. (1) and (2) are as follows:

$$\psi_a(\eta_a,\xi) = \theta_a(\eta_a,\xi) + \phi_a(\eta_a,\xi) \tag{12}$$

$$\psi_b(\eta_b,\xi) = \theta_b(\eta_b,\xi) + \phi_b(\eta_b,\xi) \tag{13}$$

2.1. Asymptotic solution of inhomogeneous boundary conditions

The governing equations with inhomogeneous boundary conditions can be written as similar to Eqs. (1) and (2)

$$\frac{\partial^2 \theta_a(\eta_a,\xi)}{\partial \eta_a^2} = \left(\frac{v_a(\eta_a)W_a^2}{\alpha LGz}\right)\frac{\partial \theta_a(\eta_a,\xi)}{\partial \xi} \tag{14}$$

$$\frac{\partial^2 \theta_b(\eta_b,\xi)}{\partial \eta_b^2} = \left(\frac{v_b(\eta_b)W_b^2}{\alpha LGz}\right)\frac{\partial \theta_b(\eta_b,\xi)}{\partial \xi} \tag{15}$$

$$\frac{\partial \theta_a(0,\xi)}{\partial \eta_a} = -\Delta \tag{16}$$

$$\frac{\partial \theta_b(0,\xi)}{\partial \eta_b} = -(1-\Delta) \tag{17}$$

$$\theta_a(1,\xi) = \theta_b(1,\xi) \tag{18}$$

$$\frac{\partial \theta_a(1,\xi)}{\partial \eta_a} = -\frac{\Delta}{1-\Delta}\frac{\partial \theta_b(1,\xi)}{\partial \eta_b} \tag{19}$$

While the fluid is sufficiently far downstream from the inlet, one can expect that the temperature profile of the fluid in the radial direction is unchanged and increased linear in ξ under the constant heat fluxes on the walls. Hence, it seems reasonable to take the asymptotic solutions of $\theta_a(\eta_a,\xi)$ and $\theta_b(\eta_b,\xi)$ as follows:

$$\theta_a(\eta_a,\xi) = \alpha_1\xi + H_a(\eta_a) \tag{20}$$

and

$$\theta_b(\eta_b,\xi) = \beta_1\left(\frac{1}{Gz} - \xi\right) + H_b(\eta_b) \tag{21}$$

Substituting Eqs. (20) and (21) into Eqs. (14) and (15) and integrating twice of the resultant equations give

$$\theta_a(\eta_a,\xi) = \alpha_1\xi + \alpha_1\Delta\left(\eta_a^3 - \frac{1}{2}\eta_a^4\right) + \alpha_2\ln\eta_a + \alpha_3 \tag{22}$$

$$\theta_b(\eta_b,\xi) = \beta_1\left(\frac{1}{Gz} - \xi\right) + \beta_1(1-\Delta)\left(\eta_b^3 - \frac{1}{2}\eta_b^4\right) + \beta_2\eta_b + \beta_3 \tag{23}$$

in which α_1 and β_1 are the undetermined constants and α_2, α_3, β_2 and β_3 are the integration constants.

2.2. Eigenfunction expansions of the homogeneous problem

The governing equations of the homogeneous problem are exactly the same as Eqs. (14) and (15) except that the homogeneous solution $\phi_a(\eta_a,\xi)$ and $\phi_b(\eta_b,\xi)$ have been incorporated with the corresponding boundary conditions are

$$\frac{\partial\phi_a(0,\xi)}{\partial\eta_a}=0 \tag{24}$$

$$\frac{\partial\phi_b(0,\xi)}{\partial\eta_b}=0 \tag{25}$$

$$\phi_a(1,\xi)=\phi_b(1,\xi) \tag{26}$$

$$\frac{\partial\phi_a(1,\xi)}{\partial\eta_a}=-\frac{\Delta}{1-\Delta}\frac{\partial\phi_b(1,\xi)}{\partial\eta_b} \tag{27}$$

The explicit solutions of $\phi_a(\eta_a,\xi)$ and $\phi_b(\eta_b,\xi)$ are thus obtained by applying the method of separation of variables as follows:

$$\phi_a(\eta_a,\xi)=\sum_{m=0}^{\infty}S_{a,m}F_{a,m}(\eta_a)G_m(\xi) \tag{28}$$

$$\phi_b(\eta_b,\xi)=\sum_{m=0}^{\infty}S_{b,m}F_{b,m}(\eta_b)G_m(\xi) \tag{29}$$

Substituting Eqs. (28) and (29) into the governing equations of $\phi_a(\eta_a,\xi)$ and $\phi_b(\eta_b,\xi)$ gives

$$G_m(\xi)=e^{-\lambda_m\left(\frac{1}{Gz}-\xi\right)} \tag{30}$$

$$F''_{a,m}(\eta_a)-\lambda_m\Delta(6\eta_a-6\eta_a^2)F_{a,m}(\eta_a)=0 \tag{31}$$

$$F''_{b,m}(\eta_b)-\lambda_m(1-\Delta)(6\eta_b-6\eta_b^2)F_{b,m}(\eta_b)=0 \tag{32}$$

and the boundary conditions in Eqs. (24)–(27) can be rewritten as

$$F'_{a,m}(0)=0 \tag{33}$$

$$F'_{b,m}(0)=0 \tag{34}$$

$$S_{a,m}F_{a,m}(1)=S_{b,m}F_{b,m}(1) \tag{35}$$

$$S_{a,m}F'_{a,m}(1)=-\frac{\Delta}{1-\Delta}S_{b,m}F'_{b,m}(1) \tag{36}$$

Combination of Eqs. (35) and (36) yields

$$\frac{F_{b,m}(1)}{F_{a,m}(1)}=-\frac{\Delta}{1-\Delta}\frac{F'_{b,m}(1)}{F'_{a,m}(1)} \tag{37}$$

To avoid the loss of generality, the eigenfunctions $F_{a,m}(\eta)$ and $F_{b,m}(\eta)$ are assumed to be polynomials and obtained with the aid of Eqs. (33) and (34) as follows:

$$F_{a,m}(\eta)=\sum_{n=0}^{\infty}d_{mn}\eta^n,\quad d_{m0}=1(\text{selected}),\ d_{m1}=0 \tag{38}$$

$$F_{b,m}(\eta)=\sum_{n=0}^{\infty}e_{mn}\eta^n,\quad e_{m0}=1(\text{selected}),\ e_{m1}=0 \tag{39}$$

where the coefficients d_{mn} and e_{mn} were expressed in terms of λ_m by substituting Eqs. (38) and (39) into Eqs. (31) and (32), as referred to in Appendix A. Thus, the eigenfunctions associated with the corresponding eigenvalues are obtained in Eqs. (38) and (39). The mathematical treatment of such homogeneous boundary value problem is the same as performed in our previous work [16]. Besides, the constants of $S_{a,m}$ and $S_{b,m}$ in Eqs. (28) and (29) can be calculated from orthogonality conditions when $n\neq m$:

$$W_b\int_0^1\left[\frac{W_a^2v_a(\eta_a)}{\alpha LGz}\right]S_{a,m}S_{a,n}F_{a,m}F_{a,n}\,d\eta_a + W_a\int_0^1\left[\frac{W_b^2v_b(\eta_b)}{\alpha LGz}\right]S_{b,m}S_{b,n}F_{b,m}F_{b,n}\,d\eta_b \tag{40}$$

2.3. Complete solution of a double-pass parallel-plate heat exchanger

A set of four simultaneous equations was obtained by substituting of Eqs. (22) and (23) and (28) and (29) into Eqs. (12) and (13) with the use of boundary conditions Eqs. (8)–(11) as follows:

$$\alpha_2=-\Delta \tag{41}$$

$$\beta_2=-(1-\Delta) \tag{42}$$

$$\sum_{m=0}^{\infty}S_{a,m}F'_{a,m}(\eta_a)G_m(\xi)+\alpha_1\Delta+\alpha_2 =-\frac{\Delta}{1-\Delta}\left(\sum_{m=0}^{\infty}S_{b,m}F'_{b,m}(\eta_b)G_m(\xi)+\beta_1(1-\Delta)+\beta_2\right) \tag{43}$$

$$\sum_{m=0}^{\infty}S_{a,m}F'_{a,m}(\eta_a)G_m(\xi)+\left(\alpha_1\xi+\frac{\Delta}{2}\alpha_1+\alpha_2+\alpha_3\right) =\sum_{m=0}^{\infty}S_{b,m}F_{b,m}(\eta_b)G_m(\xi)+\left(\beta_1\left(\frac{1}{Gz}-\xi\right)+\frac{(1-\Delta)\beta_1}{2}-\beta_2+\beta_3\right) \tag{44}$$

However, these six unknowns, say α_1, α_2 and α_3 for subchannel a and β_1, β_2 and β_3 for subchannel b, have to be determined and it needs two more additional equations to solve the unknowns.

The average dimensionless outlet temperature ψ_F may be calculated at the end of subchannel b by

$$\psi_F=-\int_0^1\frac{v_bW_bB}{V}\psi_b(\eta_b,0)\,d\eta_b =\sum_{m=0}^{\infty}\frac{-S_{b,m}e^{-\lambda_m/Gz}}{(1-\Delta)\lambda_m}\left\{F'_{b,m}(1)-F'_{b,m}(0)\right\} +\int_0^1(6\eta_b-6\eta_b^2)\left[\frac{\beta_1}{Gz}+\beta_1(1-\Delta)\left(\eta_b^3-\frac{1}{2}\eta_b^4\right)-(1-\Delta)\eta_b+\beta_3\right]d\eta_b \tag{45}$$

or may be examined by the overall energy balance on the whole system

$$V(0-\psi_F)=\int_0^{\frac{1}{Gz}} Gz\frac{\alpha BL}{W_a}\frac{\partial\psi_a(0,\xi)}{\partial\eta_a}\,d\xi + \int_0^{\frac{1}{Gz}} Gz\frac{\alpha BL}{W_b}\frac{\partial\psi_b(0,\xi)}{\partial\eta_b}\,d\xi \tag{46}$$

The left-hand side in Eq. (46) refers to the net outlet energy while the right-hand side is the total amount of the heat transferring from the walls into the flowing fluid. Taking Eqs. (8) and (9) into Eq. (46) gives

$$\psi_F = 2/Gz \tag{47}$$

The average dimensionless temperatures at the end of the conduit in two subchannels a and b are, respectively,

$$\psi_{aL}=\int_0^1 \frac{v_a W_a B}{V}\psi_a\left(\eta_a,\frac{1}{Gz}\right)d\eta_a = \sum_{m=0}^{\infty}\frac{S_{a,m}}{\Delta\lambda_m}\left\{F'_{a,m}(1)-F'_{a,m}(0)\right\} + \int_0^1 (6\eta_a-6\eta_a^2)\left[\frac{\alpha_1}{Gz}+\alpha_1\left(\eta_a^3-\frac{1}{2}\eta_a^4\right)-\Delta\eta_a+\alpha_3\right]d\eta_a \tag{48}$$

and

$$\psi_{bL}=-\int_0^1 \frac{v_b W_b B}{V}\psi_b\left(\eta_b,\frac{1}{Gz}\right)d\eta_b = \sum_{m=0}^{\infty}\frac{-S_{b,m}}{(1-\Delta)\lambda_m}\left\{F'_{b,m}(1)-F'_{b,m}(0)\right\} + \int_0^1 (6\eta_b-6\eta_b^2)\left[\frac{\beta_1}{Gz}+\beta_1(1-\Delta)\left(\eta_b^3-\frac{1}{2}\eta_b^4\right) - (1-\Delta)\eta_b+\beta_3\right]d\eta_b \tag{49}$$

As observed from Fig. 1, the average dimensionless temperature in Eqs. (48) and (49) are equal

$$\psi_{aL}=\psi_{bL} \tag{50}$$

Eqs. (41)–(44), (47) and (50) were used to solve the undetermined and integration constants in Eqs. (22) and (23) accordingly. Once all the undetermined constants in Eqs. (22) and (23) and coefficients in (28) and (29) were obtained, the dimensionless temperature distributions of both subchannels for a double-pass device were thus obtained in terms of the Graetz number (Gz), eigenvalues ($\lambda_{a,m}$ and $\lambda_{b,m}$), expansion coefficients ($S_{a,m}$ and $S_{b,m}$), impermeable-sheet location (Δ) and associated eigenfunctions ($F_{a,m}(\eta_a)$ and $F_{b,m}(\eta_b)$).

3. Heat-transfer efficiency enhancement

The average Nusselt number for double-pass operations was defined as

$$\overline{Nu}=\frac{\bar{h}W}{k} \tag{51}$$

where the average heat-transfer coefficient is calculated by making the energy balance around the whole system

$$\bar{h}(2BL)(\overline{T}_w-T_I)=\rho C_p V(T_F-T_I) \tag{52}$$

or

$$\bar{h}=\frac{\rho C_p V(T_F-T_I)}{(2BL)(\overline{T}_w-T_I)}=\frac{\rho C_p V}{2BL}\frac{\psi_F}{\overline{\psi}_w} \tag{53}$$

in which

$$\overline{T}_w=\frac{\overline{T}_{aw}+\overline{T}_{bw}}{2}=\frac{\int_0^{\frac{1}{Gz}}T_a(0,\xi)\,d\xi+\int_0^{\frac{1}{Gz}}T_b(0,\xi)\,d\xi}{2} \tag{54}$$

Substituting Eq. (53) into Eq. (51) gives

$$\overline{Nu}=\frac{\bar{h}W}{k}=\frac{VW}{2\alpha BL}\frac{\psi_F}{\overline{\psi}_w}=\frac{1}{\overline{\psi}_w} \tag{55}$$

Similarly, for a single-pass operation

$$\overline{Nu}_0=\frac{1}{\overline{\psi}_{0w}} \tag{56}$$

The device performance improvement by employing a double-pass operation is defined as the percent increase in heat transfer based on that in a single-pass device of the same working dimensions and operating parameters

$$I_h=\frac{\overline{Nu}-\overline{Nu}_0}{\overline{Nu}_0}=\frac{\overline{\psi}_{0w}-\overline{\psi}_w}{\overline{\psi}_w} \tag{57}$$

4. Power consumption increment

The power consumption will increase in a double-pass device by inserting an impermeable sheet inserted into a single-pass device. For simplicity to make a comparison, the friction losses caused by a joint, a diversion or a bending of a tube are neglected and only the wall friction loss is considered in the power consumption increment of double-pass operations in the present study.

The wall friction loss can be estimated by

$$\ell w_f = 2f\overline{v}^2 L/D_e \tag{58}$$

in which $\overline{v}$ and D_e are the average velocity of fluid in the conduits and the equivalent diameter of the conduits, respectively. The friction factor f is determined by $f=24/Re$ for the laminar flow in parallel-plate conduits. The power consumption of a single-pass device is determined by $P_0=V\rho\ell w_{f,0}$ while it in a double-pass device is determined by $P=V\rho(\ell w_{f,a}+\ell w_{f,b})$ which is the sum of the power consumption in both subchannels a and b. Accordingly, the power consumption increment, I_p, of a double-pass device is estimated based on the power consumption in a single-pass device as follows:

$$I_p=\frac{P-P_0}{P_0}=\frac{V\rho[\ell w_{f,a}+\ell w_{f,b}]-V\rho\ell w_{f,0}}{V\rho\ell w_{f,0}} = \frac{1}{\Delta^3}+\frac{1}{(1-\Delta^3)}-1 \tag{59}$$

5. Results and discussion

The temperature distribution of a double-pass parallel-plate heat exchanger under uniform heat fluxes was obtained by solving the energy balance equations with the aid of the linear superposition of the asymptotic solution for the inhomogeneous boundary conditions and the eigenfunctions expansion for the homogeneous part. The convergence of power series in Eqs. (38) and (39) is shown in Table 1. The results show that the two finite series of $n = 30$ and 33 agree reasonably well for the power series due to the resulting average Nusselt numbers are the same for the cases for $\Delta = 0.5$.

5.1. Temperature distribution and heat-transfer efficiency in a double-pass device

The wall temperature of a heat exchanger with constant heat fluxes is usually unknown in prior. However, it is important for an engineer to calculate the wall temperature before design a heat exchanger equipment for choosing the adequate heat exchanger materials. Hence we firstly show the dimensionless wall temperature distributions of the single- and double-pass devices with Δ and Gz as parameters in Fig. 2. The lower Gz represents the lower volumetric flow rate or longer conduit length resulting in the longer residence time of the fluid and higher outlet temperature as confirmed by Eq. (47). Therefore, in order to maintain the uniform heat flux, the higher wall temperature for employing the lower Gz is expected and the phenomenon was demonstrated in Fig. 2. The results in Fig. 2 indicate that the wall temperature varies more sharply along with the axial direction for $Gz = 1$ than that for $Gz = 10$. The influence of the impermeable-sheet location, Δ, is also illustrated in Fig. 2. The value of $\Delta = 0.5$ means that the impermeable sheet is inserted at the middle position between the two parallel plates while $\Delta < 0.5$ infers the impermeable sheet near the bottom plate and $\Delta > 0.5$ infers the impermeable sheet near the top plate. As shown in Eqs. (5) and (6), the $\overline{v}_a$ increases with decreasing Δ and the $\overline{v}_b$ increases with increasing Δ. Moreover, the heat-transfer coefficient of fluid is directly proportional to the fluid velocity and the higher heat-transfer coefficient means that the larger heat is removed from the wall. Therefore, Fig. 2 illustrates that the bottom wall temperature, $\psi_a(0,\xi)$, decreases with decreasing Δ, but the top wall temperature, $\psi_b(0,\xi)$, increases with decreasing Δ.

Fig. 3 shows the local transversal temperature distribution in subchannels a and b at $Gz\xi = 0.5$ (the middle point of the conduit) with Δ and Gz as parameters. Because of the fluid firstly feeds into subchannel a and then flows reversely into subchannel b as shown in Fig. 1, then the fluid temperature in subchannel a is lower than that in the subchannel b. It is worth to note that the temperature distribution in subchannel a is nearly parabolic curve and it is likely the exponential curve in subchannel b. This is due to the thermal resistance of the impermeable sheet is neglected and thus, the fluid in the subchannel a can receive the heat from subchannel b through the impermeable sheet. Hence, in subchannel a, the fluid is heated by the bottom wall and impermeable sheet simultaneously, and the parabolic temperature distribution is achieved. However, for subchannel b, the fluid is only heated by the top wall and delivers the heat to subchannel a, so the temperature distribution is of exponential curve. The fluid temperature is lower and more uniform for higher Gz than that for lower Gz as shown in Fig. 3. The temperature distribution can indicate that the wall temperature increases with Δ in subchannel a and decreases with Δ in subchannel b as concluded from Fig. 2 when one focuses on the point of $\eta_a = 0$ and $\eta_b = 0$ in Fig. 3.

Table 2 illustrates the calculation results of the average Nusselt number with Δ as a parameter. Nusselt number provides a measure of convection heat transfer occurring at the wall surface. As shown in Table 2, the $\overline{Nu}$ increases with increasing Gz and as Δ moves away 0.5. As referred to Eq. (55), the $\overline{Nu}$ is inversely proportional to the average wall temperature, $\overline{\psi}_w$, hence the larger $\overline{Nu}$ also implies that the lower average wall temperature will be obtained. Moreover, the heat-transfer efficiency enhancement, I_h, by employing a double-pass operation is defined as the percent increase in $\overline{Nu}$, based on that in a single-pass device of the same working dimensions and operating parameters, as shown in Eq. (57). Some calculated results of I_h are shown

Table 1
Convergence of power series in Eqs. (38) and (39) for n= 30 and 33 with $\Delta = 0.5$

Gz	n	λ_m	$S_{a,m}$	$S_{b,m}$	α_1	α_3	β_1	β_3	$\overline{Nu}$
1	30	−2.2	-8×10^{-17}	-7×10^{-18}	3.69	0.01	−1.69	4.05	0.39
	33	−2.2	-1×10^{-16}	5×10^{-18}	3.69	0.01	−1.69	4.05	0.39
10	30	−2.2	4×10^{-16}	9×10^{-17}	1.27	0.17	0.73	0.33	3.34
	33	−2.2	3×10^{-16}	8×10^{-17}	1.27	0.17	0.73	0.33	3.34
100	30	−2.2	3×10^{-16}	7×10^{-17}	1.03	0.18	0.97	0.20	5.11
	33	−2.2	-1×10^{-16}	-2×10^{-17}	1.03	0.18	0.97	0.20	5.11
1000	30	−2.2	3×10^{-15}	6×10^{-16}	1.00	0.19	1.00	0.19	5.36
	33	−2.2	-2×10^{-15}	-5×10^{-16}	1.00	0.19	1.00	0.19	5.36

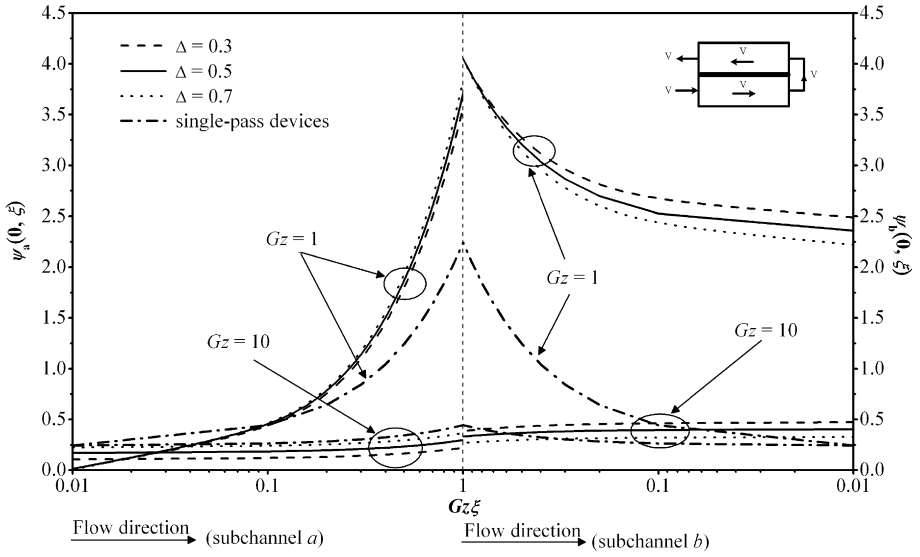

Fig. 2. Dimensionless wall temperature vs. $Gz\xi$ with Δ and Gz as parameters.

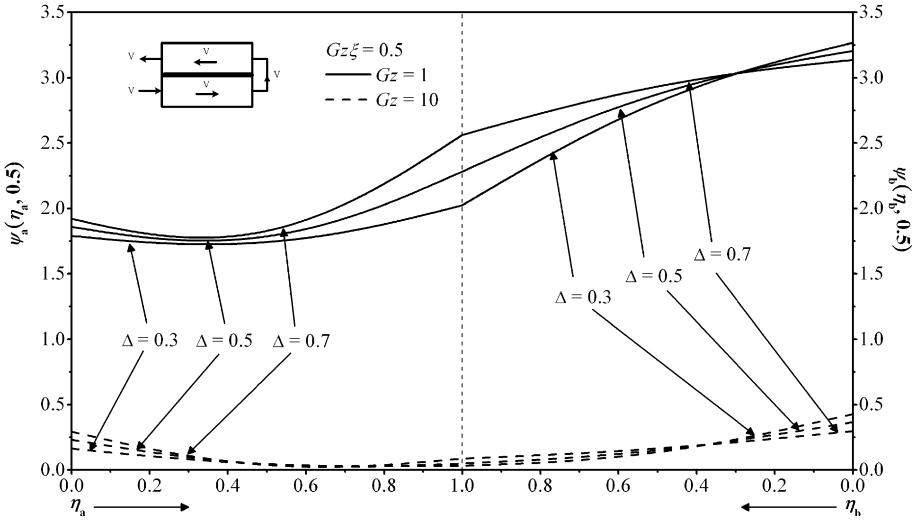

Fig. 3. The local transversal temperature in subchannels a and b with Gz as a parameter; $Gz\xi = 0.5$.

Table 2
The average Nusselt number with Δ as a parameter

$\overline{Nu}$	$\Delta = 0.1$	$\Delta = 0.3$	$\Delta = 0.5$	$\Delta = 0.7$	$\Delta = 0.9$
$Gz = 1$	0.397	0.396	0.395	0.396	0.397
$Gz = 5$	2.351	2.294	2.275	2.294	2.351
$Gz = 10$	3.510	3.383	3.343	3.383	3.510
$Gz = 50$	5.208	4.934	4.848	4.934	5.208
$Gz = 100$	5.506	5.201	5.106	5.201	5.506

Table 3
The heat-transfer efficiency enhancement with Δ as a parameter

I_h (%)	$\Delta = 0.1$	$\Delta = 0.3$	$\Delta = 0.5$	$\Delta = 0.7$	$\Delta = 0.9$
$Gz = 1$	−50.63	−50.84	−50.91	−50.84	−50.63
$Gz = 5$	4.12	1.57	0.75	1.57	4.12
$Gz = 10$	20.33	15.98	14.60	15.98	20.33
$Gz = 50$	36.90	29.68	27.44	29.68	36.90
$Gz = 100$	39.23	31.50	29.11	31.50	39.23

in Table 3. The heat-transfer efficiency enhancement, I_h, increases with increasing Gz and it is also symmetric to $\Delta = 0.5$ for fixed Gz, as observed from Table 3. The positive signs in Table 3 imply two results: (1) the heat-transfer efficiency of a double-pass device is higher than that of a single-pass device under such operating conditions; (2) a double-pass device can perform a lower average wall temperature than that in a single-pass device by employing the same operating conditions.

5.2. Power consumption increment

The double-pass operation by inserting an impermeable sheet in to an open duct not only enhance the heat-transfer

Table 4
The power consumption increment with impermeable-sheet location as a parameter

I_P				
$\Delta = 0.1$	$\Delta = 0.3$	$\Delta = 0.5$	$\Delta = 0.7$	$\Delta = 0.9$
1000.37	38.95	15	38.95	1000.37

efficiency but also increase the power consumption. As shown in Eq. (59), the power consumption increment, I_p, of a double-pass device is defined based on the power consumption in a single-pass device. The working dimensions in the calculation procedure are as follows: $L = 1.2$ m, $W = 0.04$ m, $B = 0.2$ m, $V = 1 \times 10^{-5}$ m^3/s, $\mu = 8.94 \times 10^{-4}$ kg/m s and $\rho = 997.08$ kg/m^3. The corresponding power consumption of a single-pass device is $P_0 = 2.68 \times 10^{-7}$ J/s. The calculating results of I_p are shown in Table 4. Although the maximum power consumption increment is high as 1000 for $\Delta = 0.1$ and 0.9, the corresponding power consumption is still small, say $P = 2.68 \times 10^{-4}$ J/s, and it is reasonable to ignore the power consumption in all operation conditions. An economic consideration of both the heat-transfer efficiency enhancement, I_h, and the power consumption increment, I_p, is made in the form of I_h/I_p in this study and the results are represented in Fig. 4.

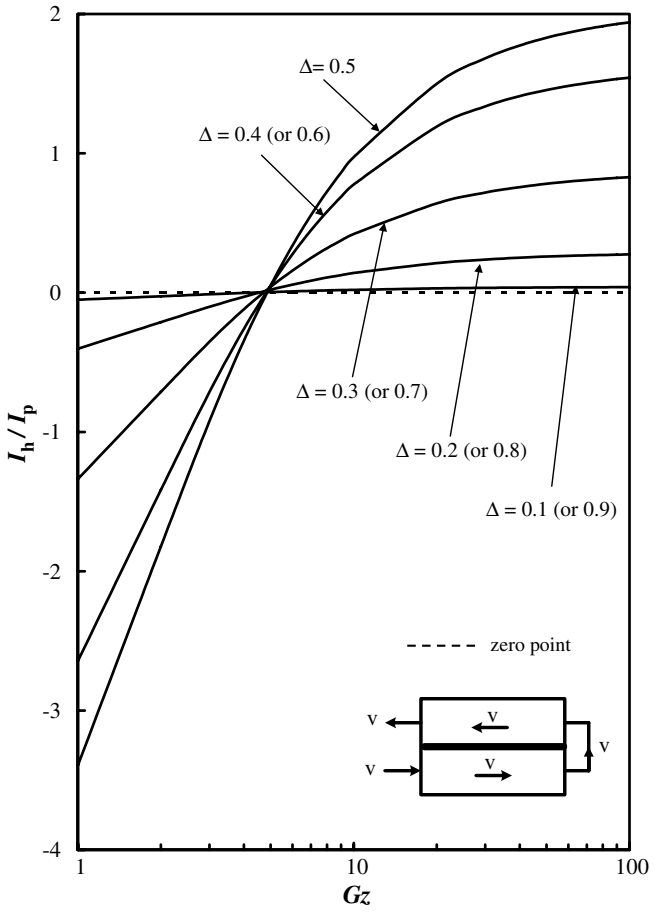

Fig. 4. The I_h/I_p with Δ as a parameter.

The dash line in the Fig. 4 is the zero point of I_h/I_p and represents that the heat-transfer efficiency of both single- and double-pass devices are equal. The lines above the dash line shows that a double-pass device has better heat-transfer efficiency than that in a single-pass device. Fig. 4 indicates that the value of I_h/I_p increases with increasing Gz and for the above the dash line range, the values of I_h/I_p increases as Δ moves away from 0.5.

6. Conclusions

The mathematical model of the heat-transfer phenomenon in a double-pass laminar countercurrent heat exchanger with uniform heat fluxes has been developed and investigated theoretically in this study. The analytical solutions for such conjugated Graetz problem are obtained by using an eigenfunction expansion in terms of power series for the homogeneous part and an asymptotic solution for the non-homogeneous part. The effects of Gz and Δ on the wall temperature, fluid temperature distributions and heat-transfer efficiency enhancement in a double-pass heat exchanger are discussed. The theoretical results show that the heat-transfer efficiency increases with increasing Gz and as Δ moves away from 0.5. The best selection of operating conditions by considering both the heat-transfer efficiency enhancement and power consumption increment, say I_h/I_p, are $Gz = 100$, $\Delta = 0.5$ as shown in Fig. 4. Moreover, the mathematical statement performed in this study can be applied to each particular application in any geometry with more general boundary conditions of multistream or multiphase problems and to predict the wall temperature distribution of the double-pass devices under uniform heat fluxes for choosing the adequate materials to build up a heat exchanger equipment.

Acknowledgment

The authors wish to thank the National Science Council of the Republic of China for its financial support.

Appendix A

Substituting the boundary conditions, Eqs. (33) and (34), into Eqs. (31) and (32) gives

$$\begin{aligned} d_{m0} &= 1 \\ d_{m1} &= 0 \\ d_{m2} &= 0 \\ d_{m3} &= \lambda_m \Delta \\ &\vdots \\ d_{mn} &= \frac{6\Delta\lambda_m(d_{mn-3} - d_{mn-4})}{n(n-1)} \end{aligned} \tag{A.1}$$

and

$$
\begin{aligned}
e_{m0} &= 1 \\
e_{m1} &= 0 \\
e_{m2} &= 0 \\
e_{m3} &= \lambda_m(1-\Delta) \\
&\vdots \\
e_{mn} &= \frac{6(1-\Delta)\lambda_m(e_{mn-3}-e_{mn-4})}{n(n-1)}
\end{aligned}
\tag{A.2}
$$

References

[1] R.K. Shah, A.L. London, Laminar Flow Forced Convection in Ducts, Academic Press, New York, 1995, pp. 196–207.

[2] P.A. Ramachandran, Boundary integral solution method for the Graetz problem, Numer. Heat Transfer, Part B 23 (1993) 257–268.

[3] A. Laouadi, N. Galanis, C.T. Nguyen, Laminar fully developed mixed convection in inclined tubes uniform heated on their outer surface, Numer. Heat Transfer, Part A 26 (1994) 719–738.

[4] M.L. Michelsen, J. Villadsen, The Graetz problem with axial heat conduction, Int. J. Heat Mass Transfer 17 (1974) 1391–1402.

[5] E. Papoutsakis, D. Ramkrishna, H.C. Lim, The extended Graetz problem with prescribed wall flux, AIChE J. 26 (1980) 779–787.

[6] B. Weigand, An extract analytical solution for the extended turbulent Graetz problem with Dirichlet wall boundary conditions for pipe and channel flows, Int. J. Heat Mass Transfer 39 (1996) 1625–1637.

[7] S. Bilir, Numerical solution of Graetz problem with axial conduction, Numer. Heat Transfer, Part A 21 (1992) 493–500.

[8] E. Papoutsakis, D. Ramkrishna, Conjugated Graetz problems. I: General formalism and a class of solid–fluid problems, Chem. Eng. Sci. 36 (1981) 1381–1390.

[9] E. Papoutsakis, D. Ramkrishna, Conjugated Graetz problems. II: Fluid–fluid problems, Chem. Eng. Sci. 36 (1981) 1393–1399.

[10] M.A. Bernier, B.R. Baliga, Conjugate conduction and laminar mixed convection in vertical pipes for upward flow and uniform wall heat flux, Numer. Heat Transfer, Part A 21 (1992) 313–332.

[11] M.R. Amin, J.A. Khan, Effects of multiple obstructions on conjugate forced convection heat transfer in tube, Numer. Heat Transfer, Part A 26 (1996) 265–279.

[12] X. Yin, H.H. Bau, The conjugated Graetz problem with axial conduction, Trans. ASME 118 (1996) 482–485.

[13] G.M. Brown, Heat or mass transfer in a fluid in laminar flow in a circular or flat conduit, AIChE J. 6 (1960) 179–183.

[14] R.J. Nunge, W.N. Gill, An analytical study of laminar counterflow double-pipe heat exchangers, AIChE J. 12 (1966) 279–289.

[15] H.M. Yeh, S.W. Tsai, C.L. Chiang, Recycle effects on heat and mass transfer through a parallel-plate channel, AIChE J. 33 (1987) 1743–1746.

[16] H.M. Yeh, C.D. Ho, The improvement of performance in parallel-plate heat exchangers by inserting in parallel an impermeable sheet for double-pass operations, Chem. Eng. Commun. 183 (2000) 39–48.

[17] C.D. Ho, H.M. Yeh, J.J. Guo, An analytical study on the enrichment of heavy water in the continuous thermal diffusion column with external refluxes, Sep. Sci. Technol. 37 (2002) 3129–3153.

[18] H.F. Zheng, X.S. Ge, Steady-state experimental study of a closed recycle solar still with enhanced falling film evaporation and regeneration, Renew. Energy 26 (2002) 295–308.

[19] M.H. Siegel, J.C. Merchuk, K. Schugerl, Air-lift reactor analysis: interrelationships between riser, downcomer, and gas–liquid separator behavior including gas recirculation effects, AIChE J. 32 (1986) 1585–1595.

[20] C.S. Bildea, A.C. Dimian, S.C. Cruz, P.D. Iedema, Design of tubular reactors in recycle systems, Comput. Chem. Eng. 28 (2004) 63–72.

[21] D. Kundu, A. Haji-Sheikh, D.Y.S. Lou, Pressure and heat transfer in cross flow over cylinders between two parallel plates, Numer. Heat Transfer, Part A 19 (1991) 345–360.

[22] D. Kundu, A. Haji-Sheikh, D.Y.S. Lou, Heat transfer predictions in cross flow over cylinders between two parallel plates, Numer. Heat Transfer, Part A 19 (1991) 361–377.

[23] C.H. Huang, M.N. Özişik, Inverse problem of determining unknown wall heat flux in laminar flow through a parallel plate duct, Numer. Heat Transfer, Part A 21 (1992) 55–70.

[24] A.V. Kuznetsov, L. Chang, M. Xiong, Effects of thermal dispersion and turbulence in forced convection in a composite parallel-plate channel: investigation of constant wall heat flux and constant wall temperature cases, Numer. Heat Transfer, Part A 42 (2002) 365–383.